MODELLING CREEP (RELAXATION) OF THE URINARY BLADDER

Nebojsa Zdravkovic[1], Mirko Rosic[2], Nikola Jankovic[1], Vladislava Stojic[1], Natasa Zdravkovic[3]
[1] Department of Medical Statistics and Informatics, Faculty of Medical Sciences, University of Kragujevac, Serbia
[2] Department of Physiology, Faculty of Medical Sciences, University of Kragujevac, Serbia
[3] Department of Internal Medicine, Faculty of Medical Sciences, University of Kragujevac, Serbia

MODELIRANJE PUZANJA (RELAKSACIJE) MOKRAĆNE BEŠIKE

Nebojša Zdravković[1], Mirko Rosić[2], Nikola Janković[1], Vladislava Stojić[1], Nataša Zdravković[3]
[1] Katedra za medicinsku statistku i informatiku, Fakultet medicinskih nauka, Univerzitet u Kragujevcu, Kragujevac, Srbija
[2] Katedra za fiziologiju, Fakultet medicinskih nauka, Univerzitet u Kragujevcu, Kragujevac, Srbija
[3] Katedra za internu medicinu, Fakultet medicinskih nauka, Univerzitet u Kragujevcu, Kragujevac, Srbija

Received / Primljen: 07. 09. 2016. Accepted / Prihvaćen: 08. 09. 2016.

ABSTRACT

We first present the results of an experiment in which the passive properties of the urinary bladder were investigated using strips of rabbit bladder. Under the assumption that the urinary bladder had orthopaedic characteristics, the strips were taken in the longitudinal and in the circumferential directions. The material was subjected to uniaxial tension, and stress-stretch curves were generated for various rates of deformation. We found that the rates did not have a significantly effect on the passive response of the material. Additionally, the stress-stretch dependence during relaxation of the material when exposed to isometric conditions was determined experimentally.

Next, we measured nonlinear stress-stretch dependence to determine the coefficients for this dependence in analytical form using a standard fitting procedure. The same approach was used to obtain the coefficients for the relaxation curves from the experimental data. Two constitutive laws, the nonlinear model for passive response and the creep model, were introduced within the shell finite element for geometrically and materially nonlinear analysis. We provide descriptions of the numerical procedures that were performed by considering the urinary bladder as a thin-walled shell structure subjected to pressure loading.

The developed numerical algorithm for the incremental-iterative solution was implemented into the finite element program, PAK. The response of the urinary bladder was calculated for continuous filling, and the numerical and experimental results were compared through cystometrograms (pressure-volume relationships). We also present comparisons of the shapes and volumes of the urinary bladder obtained numerically and experimentally. Finally, the numerical results of the creep response, when placed under constant internal pressure, are provided for various stages of deformation.

Keywords: *Urinary bladder, Passive properties, Creep of material, Finite element modelling*

SAŽETAK

Prvo predstavljamo eksperimentalno određivanje osobina mokraćne bešike u pasivnom stanju korišćenjem segmenata bešike. Uzeti su segmenti u uzdužnom i poprečnom pravcu pretpostavljajući da bešika ima ortotropne karakteristike. Izvršeno je jednoosno izduživanje materijalnih segmenata i dobijene su napon-streč krive za različite brzine deformacije. Pronađeno je da brzine nemaju značajnog efekta na odgovor materijala u pasivnom stanju. Takođe je eksperimentalno određena napon-streč zavisnost tokom relaksacije materijala izloženog izometrijskim uslovima.

Zatim smo primenili izmerene nelinearne relacije napon-streč da odredimo koeficijente ove zavisnosti u analitičkoj formi korišćenjem standardne procedure fitovanja. Isti pristup je korišćen da bi odredili koeficijente za eksperimentalno dobijene krive relaksacije. Uvedena su dva konstitutivna zakona: nelinearni model za pasivni odgovor i model puzanja, korišćenjem konačnog elementa ljuske za geometrijsku i materijalno nelinearnu analizu. Dajemo opis numeričke procedure, smatrajući mokraćnu bešiku strukturom tankozidne ljuske opterećene pritiskom.

Razvijeni algoritam za inkrementalno-iterativno rešavanje je implementiran u program za konačne elemente PAK. Proračunat je odgovor mokraćne bešike za kontinualno punjenje, i numerički i eksperimentalni rezultati su upoređeni preko cistometrograma (krivih pritisak-zapremina). Takođe predstavljamo poređenje oblika i zapremina mokraćne bešike dobijenih numerički i eksperimentalno. Konačno, prikazani su numerički rezultati puzanja bešike u slučaju konstantnog unutrašnjeg pritiska, za različite faze deformacije.

Ključne reči: *Mokraćna bešika, Pasivne osobine, Puzanje materijala, Modeliranje konačnim elementima.*

ABBREVIATIONS

FEM - Finite element modelling

PAK - Finite element program for linear and nonlinear structural analysis, mass and heat transfer and biomechanics

DE GRUYTER OPEN

UDK: 616.62-007:577.3 / Ser J Exp Clin Res 2017; 18 (4): 295-306
DOI: 10.1515/SJECR-2016-0067

Corresponding author: Vladislava Stojić
Department of Medical Statistics and Informatics; Faculty of Medical Sciences; University of Kragujevac
Svetozara Markovica 69, 34000 Kragujevac, Serbia; Telephone: 381-34-306-800; e-mail: vladislavstojic@medf.kg.ac.rs

INTRODUCTION

The passive and active mechanical properties of the urinary bladder wall have been the subject of investigation in many studies (1, 3, 5, 7, 11, 12). Based on the experimental findings of these studies, various forms of analytical expressions have been proposed to describe the material characteristics of the urinary bladder wall and the response of the urinary bladder as a whole.

Because of the combination of modern numerical methods, such as the finite element method (FEM), and contemporary computer development, simulation of the complex three-dimensional (3D) behaviour of human organs is possible. Along this line, we analysed the dynamic responses of muscle and cartilage to the mechanical loads and physiological stimuli that are extremely important for understanding the mechano-biochemical processes that occur in biological structures (8, 9, 10). Here, we focus on the passive mechanical responses of the urinary bladder.

Our numerical analysis of the urinary bladder (under passive conditions) is based on the constitutive laws of the bladder wall that have been established based on data collected in specifically designed experiments. We defined the following two FEM material models: 1) a model for nonlinear material response derived based on the measured stress-stretch relationship; and 2) a creep material model derived based on experimental relaxation data. We modelled the urinary bladder as a shell structure undergoing large displacements and calculated the passive response of the urinary bladder. Specifically, we focused on the pressure-volume relationship (cystometrogram) and the rate of the volume change due to material creep. The predictions generated for whole organ response were compared with experimentally obtained cystometrogram data.

2. EXPERIMENTAL PROTOCOL

A total number of 20 rabbits of both sexes that weighed approximately 2.5-3 kg was used. All animals were killed by cervical dislocation according to Schedule 1 of the Animal (Scientific Procedures) Act, 1986, UK. The urinary bladders of the rabbits were emptied and dissected out, and strips of bladder were placed in an organ chamber perfused with Krebs-Ringed solution (in mM, NaCl 117, KCl 4.7, $NaHCO_3$ 24.8, $MgSO_4$ x $7H_2O$ 1.2, $CaCl_2$ 2.5, KH_2PO_4 1.2 and D-glucose 11.1). The solution was continuously bubbled with a mixture of 95% O_2 and 5% CO_2 and maintained at 31±1 °C to prevent spontaneous contractions. Different initial strip lengths were taken in the longitudinal and circumferential directions and strained continuously using various strain rates. Developed force was measured using an isotonic transducer (Elunit, Yugoslavia) and recorded using a PIC digital recording system (ECM, Yugoslavia). We allowed the strips to relax after various initial stretches were performed to measure relaxation under isometric conditions. We defined the strip length measured just before visible changes in tension were recorded on the PIC digital recording system as the initial length.

The filling pressure-volume curve of the urinary bladder, known as a cystometrogram (CMG), was determined by increasing the contained volume and measuring the pressure response. We used two experimental protocols to generate the cystometrograms for isolated bladders. During the first experiment, the bladders were emptied, dissected out, transferred to oxygenated Krebs-Ringer solution, and filled continuously at a velocity of 4.8 ml/min using a slow drive syringe pump (syringe pump mod 355/ Sage instr.). During the second experiment, the bladders were filled with Krebs-Ringer solution in a stepwise manner, with increases of 10 ml occurring at 20-second increments. Pressure responses were measured using a pressure transducer (Ugo Basile, USA) and recorded using a PIC digital recording system (ECM, Serbia).

3. FINITE ELEMENT MODELLING

The geometry of the urinary bladder can be closely approximated using a thin-walled shell type structure. Naturally, shell finite elements are most appropriate when generating finite element models, as shown in Fig. 1. In this article, we also describe the numerical procedures used for calculating urinary bladder responses under passive conditions using the results of the experimental investigation described in Section 2.

We assessed the large strain and large displacement formulation of the shell finite elements (2). Since our material model was based on stress-stretch curves, we first provide some necessary equations that describe the kinematics of deformation and then describe the implementation of the material models.

In nonlinear finite element analysis, the equilibrium equation is formulated as follows:

$$ {}^{t+\Delta t}\mathbf{K}^{(i-1)}\Delta\mathbf{U}^{(i)} = {}^{t+\Delta t}\mathbf{F}^{ext} - {}^{t+\Delta t}\mathbf{F}_{\text{int}}^{(i-1)} \qquad (1) $$

where is the incremental nodal displacement vector ${}^{t+\Delta t}\mathbf{K}^{(i-1)}$ is the element stiffness matrix ${}^{t+\Delta t}\mathbf{F}^{\mathbf{ext}}$ and ${}^{t+\Delta t}\mathbf{F}_{\text{int}}^{(i-1)}$ are the external and internal nodal forces, respectively; the t+Dt index denotes the end of time (load) step; and "i" represents the equilibrium iteration number for the current time step. The stiffness matrix and nodal forces were expressed as follows:

$$ {}^{t+\Delta t}\mathbf{K}^{(i-1)} = \int_V {}^{t+\Delta t}\mathbf{B}_{\mathbf{L}}^{(i-1)T}\ {}^{t+\Delta t}\mathbf{C}^{(i-1)}\ {}^{t+\Delta t}\mathbf{B}_{\mathbf{L}}^{(i-1)}\mathbf{dV} + \int_V {}^{t+\Delta t}\mathbf{B}_{\mathbf{NL}}^{(i-1)T}\ {}^{t+\Delta t}\hat{\sigma}^{(i-1)}\ {}^{t+\Delta t}\mathbf{B}_{\mathbf{NL}}^{(i-1)}\mathbf{dV} \qquad (2) $$

$$ {}^{t+\Delta t}\mathbf{F}_{\text{int}}^{(i-1)} = \int_V {}^{t+\Delta t}\mathbf{B}_{\mathbf{L}}^{(i-1)T}\ {}^{t+\Delta t}\sigma^{(i-1)}\mathbf{dV} \qquad (3) $$

where $\mathbf{B}_L$ and $\mathbf{B}_{NL}$ are the linear and nonlinear strain-displacement transformation matrices, $\mathbf{C}$ is the constitutive

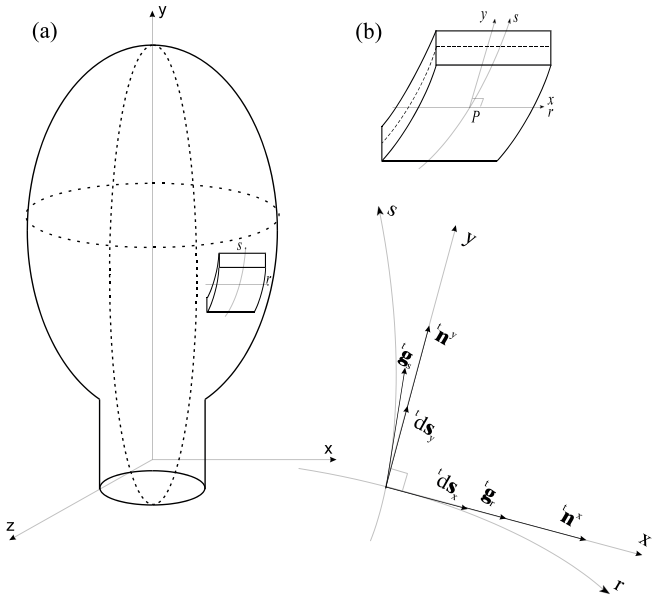

Fig. 1 Urinary bladder model
(a) Urinary bladder as a thin-walled structure
(b) Shell finite element with the principal material axes

matrix (stress-strain matrix); and $\hat{\sigma}$ and σ are the matrix and vector of the stress components for the indicated time step and iteration, respectively. $\mathbf{B}_L$ and $\mathbf{B}_{NL}$ were calculated using a standard procedure (2) and the formulation of the shell finite elements.

For the shell finite element analysis, the local coordinate system (x-y) was defined in the shell tangential plane, as shown in Fig. 1. The x-axis was taken as the direction of the (first) r-axis along the natural coordinate line, while "y" was orthogonal to the x-axis. For the current configuration (we omitted the index for iteration number to simplify the notation), we determined the rate of stretch (${}^{t+\Delta t}_{0}\lambda_x$) in the x direction using the following equations. The lengths of a material element on the r-line at time t+Dt and t=0 (Fig. 1(b)) are as follows:

$$ {}^{t+\Delta t}ds_x = \left\| {}^{t+\Delta t}d\mathbf{s}_x \right\| = \left\| \frac{\partial \mathbf{x}}{\partial \mathbf{r}} dr \right\| = \left\| {}^{t+\Delta t}\mathbf{g}_r \right\| dr \tag{4} $$

$$ {}^{0}ds_x = \left\| {}^{0}d\mathbf{s}_x \right\| = \left\| {}^{0}\mathbf{g}_r \right\| dr = \left\| {}^{0}\mathbf{J}_1 \right\| dr \tag{5} $$

where ${}^{t+\Delta t}\mathbf{g}_r$ and ${}^{0}\mathbf{g}_r$ were the base vectors of the r-curve at the current and initial configurations, respectively; and ${}^{t+\Delta t}\mathbf{J}_1$ and ${}^{0}\mathbf{J}_1$ were the first rows in the Jacobian matrix of the following coordinate transformation: $\mathbf{J} = \partial \mathbf{x} / \partial \mathbf{r}$. The rate of stretch ${}^{t+\Delta t}_{o}\lambda_x$ was determined using the following equation:

$$ {}^{t+\Delta t}_{o}\lambda_x = \frac{\left\| {}^{t+\Delta t}\mathbf{g}_r \right\|}{\left\| {}^{0}\mathbf{g}_r \right\|} = \frac{\left\| {}^{t+\Delta t}\mathbf{J}_1 \right\|}{\left\| {}^{0}\mathbf{J}_1 \right\|} \tag{6} $$

The rate of stretch (${}^{t+\Delta t}_{o}\lambda_x$) can also be calculated as follows:

$$ {}^{t+\Delta t}_{0}\lambda_x = \sqrt{ {}^{t+\Delta t}_{0}C_{ij} \; {}^{0}n_i^x \; {}^{0}n_j^x } \tag{7} $$

where ${}^{t+\Delta t}_{0}C_j$ is the right Cauchy-Green deformation tensor

$$ ({}^{t+\Delta t}_{0}\mathbf{C} = {}^{t+\Delta t}_{0}\mathbf{F}^{T} \; {}^{t+\Delta t}_{0}\mathbf{F}) \tag{8} $$

and ${}^{0}\mathbf{n}^{x}$ is the normal vector in the x direction within the reference configuration. Additionally, ${}^{t+\Delta t}_{0}\mathbf{F} \hat{=} {}^{t+\Delta t}\mathbf{x}/\partial {}^{0}\mathbf{x}$ is the deformation gradient. The stretch in the orthogonal "y"-direction is determined by using definition vectors ${}^{t+\Delta t}d\mathbf{s}_y$ and ${}^{0}d\mathbf{s}_y$ in the y direction as follows:

$$ {}^{t+\Delta t}d\mathbf{s}_y = {}^{t+\Delta t}\mathbf{g}_y \, dr = \left\{ ({}^{t+\Delta t}\mathbf{g}_y)_X \, \mathbf{i} + ({}^{t+\Delta t}\mathbf{g}_y)_Y \, \mathbf{j} + ({}^{t+\Delta t}\mathbf{g}_y)_Z \, \mathbf{k} \right\} dr \tag{9} $$

$$ {}^{0}d\mathbf{s}_y = {}^{0}_{t+\Delta t}\mathbf{F} \; {}^{t+\Delta t}d\mathbf{s}_y = {}^{0}_{t+\Delta t}\mathbf{F} \; {}^{t+\Delta t}\mathbf{g}_y \, dr \tag{10} $$

$$ \text{as } {}^{t+\Delta t}_{0}\lambda_y = \frac{ {}^{t+\Delta t}ds_y }{ {}^{0}ds_y } = \frac{ \left\| {}^{t+\Delta t}\mathbf{g}_y \right\| }{ \left\| {}^{0}_{t+\Delta t}\mathbf{F} \; {}^{t}\mathbf{g}_y \right\| } \tag{11} $$

where ${}^{0}_{t+\Delta t}\mathbf{F} = {}^{t+\Delta t}_{0}\mathbf{F}^{-1}$ is the inverse deformation gradient and

$$ {}^{t+\Delta t}\mathbf{g}_y = {}^{t+\Delta t}\mathbf{n} \times {}^{t+\Delta t}\mathbf{g}_r \tag{12} $$

is the base vector in the "y" direction; ${}^{t+\Delta t}\mathbf{n}$ is the shell normal. Additionally, the following equation may be derived based on equation (7):

$$ {}^{t+\Delta t}_{0}\lambda_y = \sqrt{ {}^{t+\Delta t}_{0}C_{ij} \; {}^{0}n_i^y \; {}^{0}n_j^y } \tag{13} $$

The numerical results for the stretches calculated using the base vectors and the Cauchy-Green deformation tensor were the same, but the first approach was more computationally efficient. The stretch (λ_z) occurring in the shell normal direction was determined based on the incompressibility condition of the material as follows:

$$ \lambda_z = \lambda_x^{-1} \, \lambda_y^{-1} \tag{14} $$

Using the λ_z calculated using the previous equation, we calculated the current shell thickness (${}^{t+\Delta t}h$) using the following equation:

$$ {}^{t+\Delta t}h = {}^{0}h \; {}^{t+\Delta t}_{o}\lambda_z \tag{15} $$

where ${}^{0}h$ is the initial thickness.

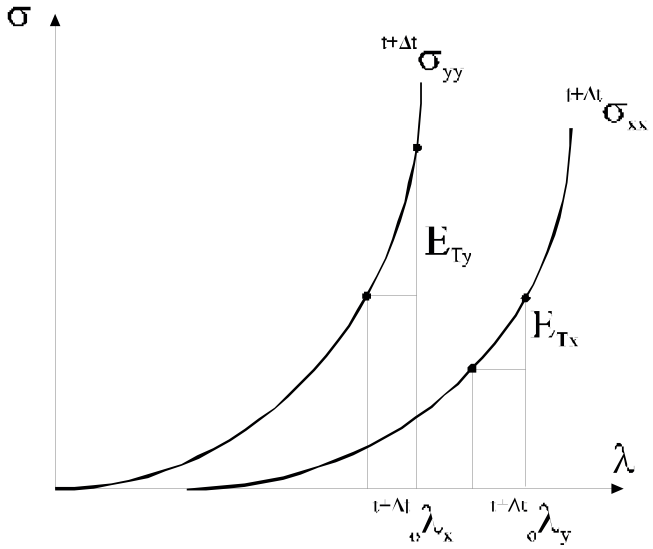

Fig. 2 Schematic representation of the material characteristics curves

3.1 THE STRESS-STRETCH MATERIAL MODEL

The stress calculated herein represents the Cauchy stress (force per unit current area). In accordance with the literature data and results of our experimental investigation, we introduced several basic assumptions to be used when formulating the material model. The assumptions were as follows:

a) The material was orthotropic;
b) The material was incompressible, as indicated by the identification of a Poisson's ratio of $\nu \approx 0.5$ in all directions; and
c) The normal stresses were dominant in the material.

The axially symmetric structure under axially symmetric loading conditions was evaluated by establishing the x-axis in the circumferential direction and "y" in the axial direction. Additionally, in accordance with assumption a), we used the experimental curves (Fig. 2) generated in these two orthogonal directions. The observations we made during the experiments suggested that the lateral strain placed on the strips during uniaxial straining was practically the same, so the model met assumption b).

The normal stresses ${}^{t+\Delta t}\sigma_x$ and ${}^{t+\Delta t}\sigma_y$ were determined according to the following procedure. First, we write notated the strains corresponding to the stress increments as follows:

$$de_{xx} = \frac{d\sigma_{xx}}{E_x} - \nu\frac{d\sigma_{yy}}{E_y} \tag{16}$$

$$de_{yy} = -\nu\frac{d\sigma_{xx}}{E_x} + \frac{d\sigma_{yy}}{E_y} \tag{17}$$

where Ex and Ey are the tangent moduli that can be expressed as

$$E_x = \frac{d\sigma_{xx}}{de_{xx}} = \frac{d\sigma_{xx}}{d\lambda_x}\frac{d\lambda_x}{de_{xx}} = E_{Tx}\ {}^t_o\lambda_x \tag{18}$$

$$E_y = \frac{d\sigma_{yy}}{de_{yy}} = \frac{d\sigma_{yy}}{d\lambda_y}\frac{d\lambda_y}{de_{yy}} = E_{Ty}\ {}^t_o\lambda_y \tag{19}$$

Here, ETx and ETy were the tangent moduli to the stress-stretch curves shown in Fig. 2. We employed the following equation to derive the aforementioned relationships:

$$d\lambda = \lambda\, de \tag{20}$$

based on the definitions for stretch (l) and small strain €. The stress-stretch curves were approximated using the constitutive laws as follows:

$$\sigma_{xx} = a_x\left(\frac{1}{b_x}(({}^t_o\lambda_x)^{b_x} - 1)\right) = a_x\, g_x({}^t_o\lambda_x) \tag{21}$$

$$\sigma_{yy} = a_y\left(\frac{1}{b_y}(({}^t_o\lambda_y)^{b_y} - 1)\right) = a_y\, g_y({}^t_o\lambda_y) \tag{22}$$

where a_x, b_x, a_y, b_y are the coefficients identified by fitting the analytical expressions to the experimental curves. We noted that the functions for $g(\lambda)$ satisfied the defined conditions necessary for reducing the stretch applied to small strain tensors in cases of small stretch as follows:

$$g(1) = 0 \tag{23}$$

$$\left(\frac{\partial g}{\partial \lambda}\right)_{\lambda_i=1} = g'(1) = 1 \tag{24}$$

Based on equations (16) and (17), we solved for the stress increments as follows:

$$\begin{Bmatrix} d\sigma_x \\ d\sigma_y \end{Bmatrix} = \frac{1}{1-\nu^2}\begin{bmatrix} E_{\bar{x}} & \nu\frac{{}^t_o\lambda_x}{{}^t_o\lambda_y}E_{\bar{x}} \\ \nu\frac{{}^t_o\lambda_y}{{}^t_o\lambda_x}E_{\bar{y}} & E_{\bar{y}} \end{bmatrix}\begin{Bmatrix} d\lambda_x \\ d\lambda_y \end{Bmatrix} \tag{25}$$

The stress increments in time step were defined as follows:

$$\begin{Bmatrix} d\sigma_x \\ d\sigma_y \end{Bmatrix} = \frac{1}{1-\nu^2}\begin{bmatrix} E_{\bar{x}} & \nu\frac{{}^t_o\lambda_x}{{}^t_o\lambda_y}E_{\bar{x}} \\ \nu\frac{{}^t_o\lambda_y}{{}^t_o\lambda_x}E_{\bar{y}} & E_{\bar{y}} \end{bmatrix}\begin{Bmatrix} d\lambda_x \\ d\lambda_y \end{Bmatrix} \tag{26}$$

$$\Delta\sigma_y = \frac{1}{1-\nu^2}\left(\int_t^{t+\Delta t}\nu\frac{{}^\tau_o\lambda_y}{{}^\tau_o\lambda_x}E_{\bar{y}}\ d\lambda_x + \int_t^{t+\Delta t}E_{\bar{y}}\ d\lambda_y\right) \tag{27}$$

Using the expressions for stress-stretch curves (equations (21) and (22)), we obtained the following equations:

$$\Delta\sigma_{xx} = \frac{1}{1-\nu^2}\left(a_x \frac{1}{b_x}\left(\left({}^{\tau}_{o}\lambda_x\right)^{b_x} - 1\right) + \nu\left(\lambda_x E_{Tx}\right)_{mean} \ln\left({}^{\tau}_{o}\lambda_y\right)\right) \quad (28)$$

$$\Delta\sigma_{xx} = \frac{1}{1-\nu^2}\left(a_x \frac{1}{b_x}\left(\left({}^{\tau}_{o}\lambda_x\right)^{b_x} - 1\right) + \nu\left(\lambda_x E_{Tx}\right)_{mean} \ln\left({}^{\tau}_{o}\lambda_y\right)\right)_{t}^{t+\Delta t} \quad (29)$$

in which we have employed the following approximations:

$$\lambda_{mean} = \frac{1}{2}\left({}^{t}_{o}\lambda + {}^{t+\Delta t}_{o}\lambda\right) \quad (30)$$

$$E_{Tmean} = \frac{1}{2}\left({}^{t}E_T + {}^{t+\Delta t}E_T\right) \quad (31)$$

Therefore, the following stresses were identified at the end of time (load) step:

$${}^{t+\Delta t}\sigma_{xx} = {}^{t}\sigma_{xx} + \Delta\sigma_{xx} \quad (32)$$

$${}^{t+\Delta t}\sigma_{y} = {}^{t}\sigma_{y} + \Delta\sigma_{y} \quad (33)$$

When $\lambda < 1$, we used the constitutive relations defined for $\lambda > 1$.

In accordance with assumption c), we calculate the shear modulus (G) as follows:

$$G = \frac{E_x + E_y}{4(1+\nu)} \quad (34)$$

which reduced the isotropic value when $E_x = E_y$. The shear stresses were determined using the Green-Lagrange shear strains, which were calculated in the standard manner (2).

3.2 CREEP MODEL

As previously described in Section 2, the creep behaviour of the material was determined via relaxation tests. We obtained a family of relaxation curves via the relaxation tests, which are shown schematically in Fig. 3. These curves can be approximated by the following expression:

$$\sigma = c_0 + c_1 e^{c_2 t} \quad (35)$$

where $c_0 = c_0(\lambda)$, $c_1 = c_1(\lambda)$, and $c_2 = c_2(\lambda)$ were the material parameters that were obtained by fitting of this equation to the experimental results.

After taking into account the creep effect at time step Dt, we proceeded as follows. The total normal stress ${}^{t+\Delta t}\sigma$ (in direction x or y) was expressed as follows:

$$\sigma = c_0 + c_1 e^{c_2 t} \quad (36)$$

where ${}^{t+\Delta t}\sigma^{t}$ is the level of stress corresponding to the transient response, and $\Delta\sigma^{c}$ represents the contribution

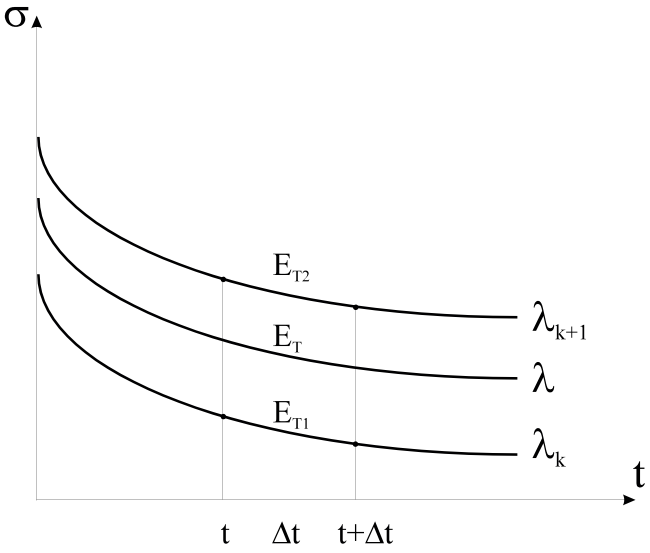

Fig. 3 Relaxation curves for various stretches λ

of the creep effect. The creep stress $\Delta\sigma^{c}$ was determined using the following equation:

$$\sigma = c_0 + c_1 e^{c_2 t} \quad (37)$$

where E_T is the slope on the relaxation curve given stretch l. The modulus E_T was interpolated based on the two measured curves (with $\lambda_k \le \lambda$ and $\lambda_{k+1} \ge \lambda$) as follows:

$$E_T = E_{T1} + \frac{E_{T2} - E_{T1}}{\lambda_{k+1} - \lambda_k}\left(\lambda - \lambda_k\right) \quad (38)$$

where E_{T1} and E_{T2} were the moduli on the curves with λ_k and λ_{k+1},

$$E_{T1} = \left(\frac{d\sigma}{dt}\right)_{\lambda=\lambda_k} = c_{11}\, c_{21}\, e^{c_{21} t} \quad (39)$$

$$E_{T2} = \left(\frac{d\sigma}{dt}\right)_{\lambda=\lambda_{k+1}} = c_{12}\, c_{22}\, e^{c_{22} t} \quad (40)$$

in which coefficients c_1, c_2 and c_2, c_2 corresponded to the curves with λ_k and λ_{k+1}, respectively.

We used the current stretch l at a given material point as the mean value identified in the current time step, as follows:

$$\lambda = \frac{1}{2}\left({}^{t}\lambda + {}^{t+\Delta t}\lambda\right) \quad (41)$$

In the proposed creep model, we did not take into consideration the creep effects on the shear modulus since normal stress/strain components are the main contributors to urinary bladder response.

4. EXPERIMENTAL RESULTS

In this section, we present the results of the experiments described in Section 2 that used the rabbit urinary bladder

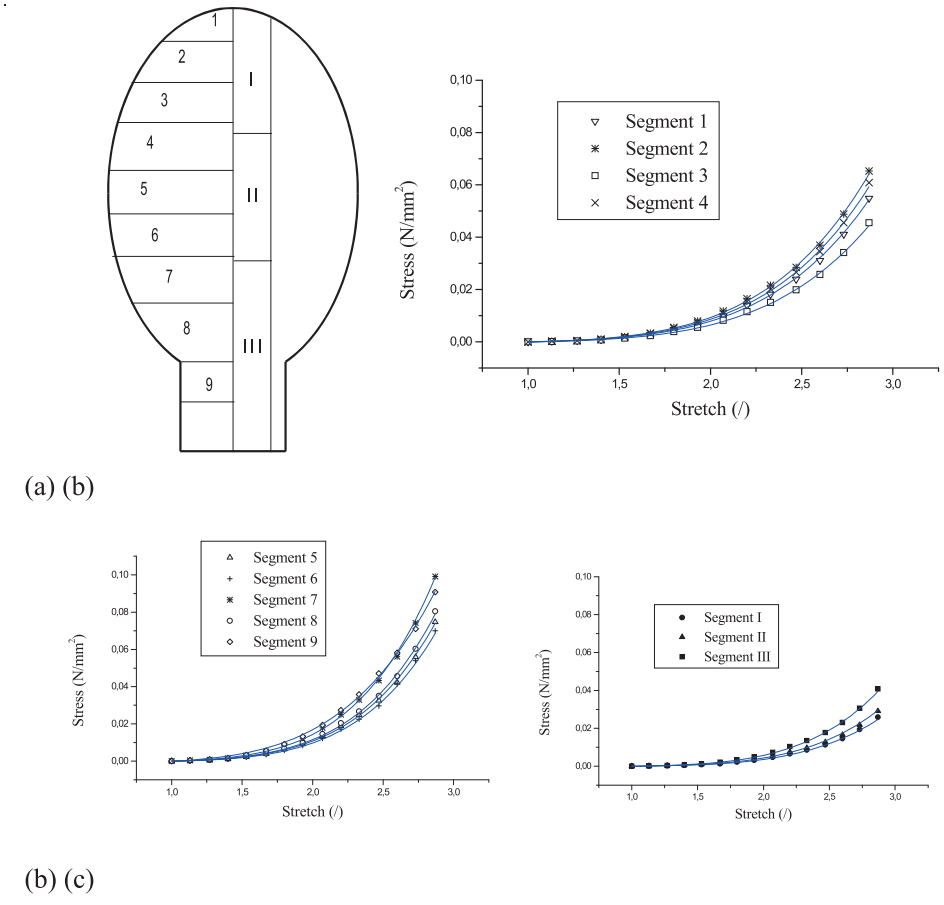

Fig. 4 Stress-stretch curves for various segments
(a) Schematic view of the urinary bladder with segments
(b) Stress-stretch dependence in the longitudinal direction
(c) Stress-stretch dependence in the circumferential direction

strips. First, we provide four typical stress-stretch curves from which the important conclusions regarding the mechanical characteristics of the material were drawn and then we present two relaxation curves. Additionally, we illustrate the mechanical behaviour of the urinary bladder using cystometrograms for continuous and stepwise loading. Based on the range of the experimentally derived strain rates $(0.5\,s^{-1} - 8\,s^{-1})$, we found that the strain rate effects could be neglected.

Longitudinal			Circumferential		
Segment	ay	by	Segment	ax	bx
I	0.0008	5.2818	1	0.0011	5.2818
II	0.0006	5.2818	2	0.0013	5.2818
III	0.0005	5.2818	3	0.0009	5.2818
			4	0.0012	5.2818
			5	0.0015	5.2818
			6	0.0013	5.3759
			7	0.0020	5.2818
			8	0.0016	5.2818
			9	0.0034	4.5690

Table 1 Constitutive coefficients for the longitudinal and circumferential directions

The nonhomogeneous and orthotropous character of the urinary bladder wall material is shown in Fig. 4. Material segments in the longitudinal and circumferential directions were taken from various positions in the urinary bladder, as shown in Fig. 4a. Based on Figs. 4b and c, one can observe that the segments in the lower part of the bladder demonstrated stiffness in both directions. Additionally, the stiffness identified in the circumferential direction was higher than the stiffness identified in the longitudinal direction. The continuous curves in these figures correspond to the equations (21) and (22), while the discrete points represent the experimental values. Table 1 provides the values of material constants "a" and "b", which were obtained using a standard curve fitting procedure.

As described in Sections 2 and 3, the creep behaviour of the material was represented via the relaxation curves. These curves were obtained by stretching the specimens to stretch l and then holding the strain constant and measuring the forces during relaxation time. Figs. 5a and 5b illustrate the relaxation curves for the longitudinal and circumferential directions, wherein the solid lines correspond to the analytical expression (36), and the experimental results are represented by the discrete points. Based on these figures, we observed that the amount of the stress relaxation

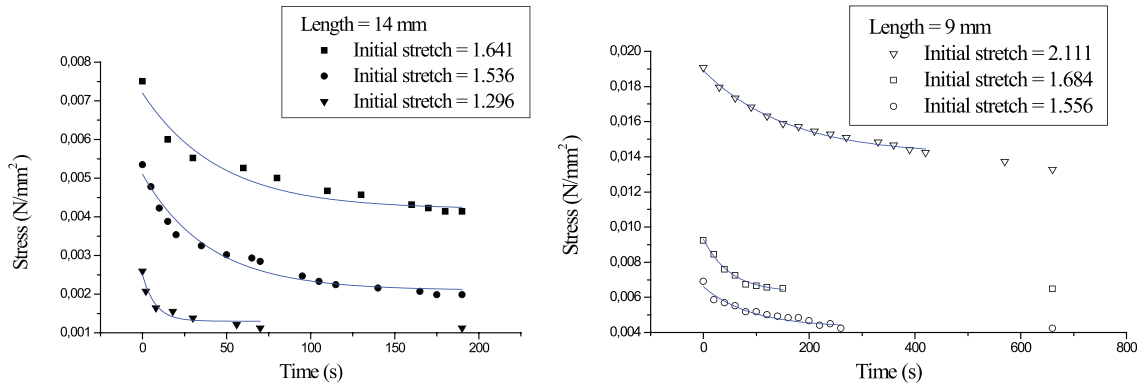

Fig. 5 Stress relaxation
(a) Longitudinal segments (solid symbols)
(b) Circumferential segments (open symbols)

Longitudinal				Circumferential			
Stretch	c0	c1	c2	Stretch	c0	c1	c2
1.641	0.0042	0.0030	-0.0220	2.111	0.0141	0.0048	-0.0063
1.536	0.0021	0.0030	-0.0253	1.684	0.0063	0.0030	-0.0198
1.296	0.0013	0.0012	-0.1297	1.556	0.0043	0.0023	-0.0111

Table 2 Coefficients derived for the longitudinal and circumferential directions using the creep model

was within approximately 40% of the initial stress levels. The material coefficients for the relaxation curves are provided in Table 2.

Finally, Fig. 6 shows the pressure-volume curves (cystometrograms) that were derived for the continuous and stepwise fillings using the procedures described in Section 2. The recorded pressure-volume curves had the same general nonlinear character as the uniaxial stress-stretch relationships observed for the bladder strips. Additionally, no significant difference was observed between the responses observed during the continuous and stepwise fillings, indicating that the creep contribution to the intervals of constant pressure was not high.

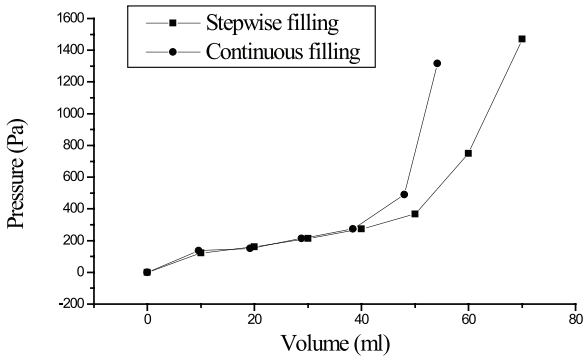

Fig. 6 Pressure-volume dependence (cystometrogram) for the continuous and stepwise fillings

5. NUMERICAL SIMULATIONS

During the numerical simulations, we demonstrated the accuracy of the numerical models when compared with experimental results by considering the whole urinary bladder as a structure and via a simple creep problem.

Uniaxial Stretch.

This example serves to demonstrate the accuracy of the numerical procedure and the calculated material response when compared with the experimental observations. The following two extreme cases are considered:

a) the material was free to contract laterally; and
b) the material was restrained in the lateral direction.

Fig. 7a shows the one four-node shell finite element with dimensions, boundary conditions and loading included in the analysis. The element was loaded with stress ${}^{t+\Delta t}\sigma_x$ that increased over time, as shown in Fig. 7b. The constitutive curves generated under the assumption that the material was orthopaedic are shown in Fig. 7c. The solutions were obtained using (1) one-step solution (Dt=1s, Dt=2s,..., Dt=6s) from the zero-stress to the current stress, and (2) multistep solution, with Dt=1 ranging from time t=0 to the current time (t=,1 s, t=2s, ..., t=6s). We observed that the one-step and multistep solutions displayed good accuracy. Additionally, the numerical solutions ${}^{t+\Delta t}\sigma_x(\lambda_x)$ laid approximately on the analytical curves for both isotropic and orthotropic material, while

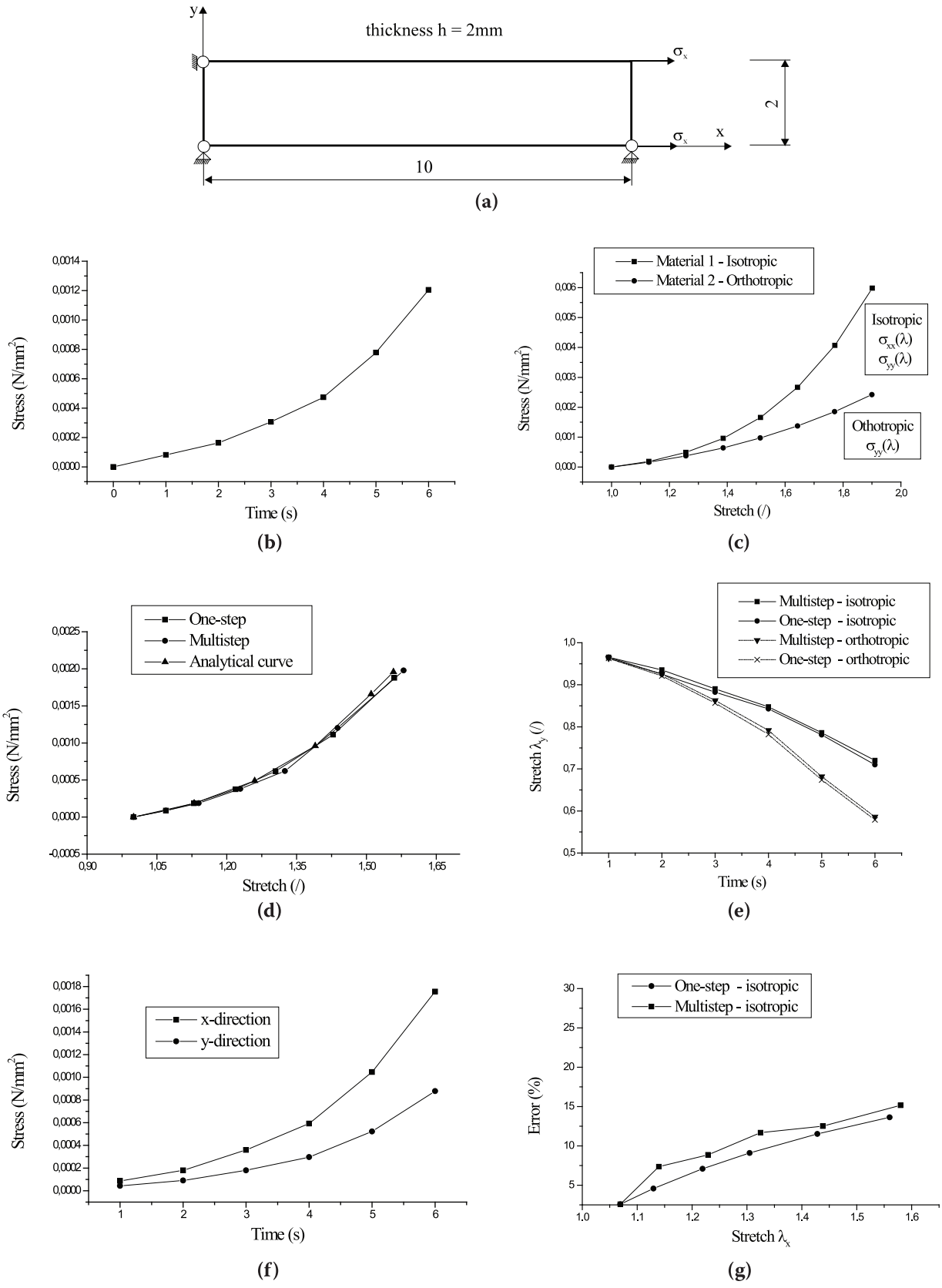

Fig. 7 Uniaxial stretch
(a) Shell finite element
(b) Stress-time relationship (prescribed)
(c) Stress-stretch relationships (prescribed)
(d) Stress-stretch numerical solution
(e) Stretch-time dependence in the y direction (computed)
(f) Stress-time dependence in the x and y directions (computed)
(g) Error- stretch dependence in the x direction (computed)

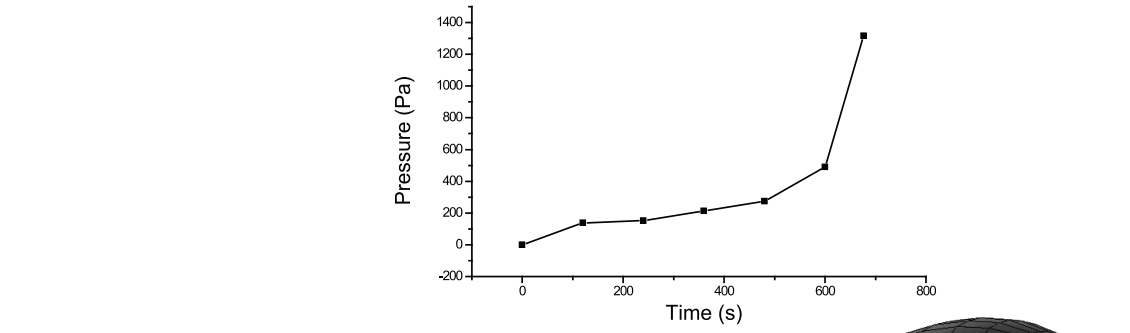

(a)

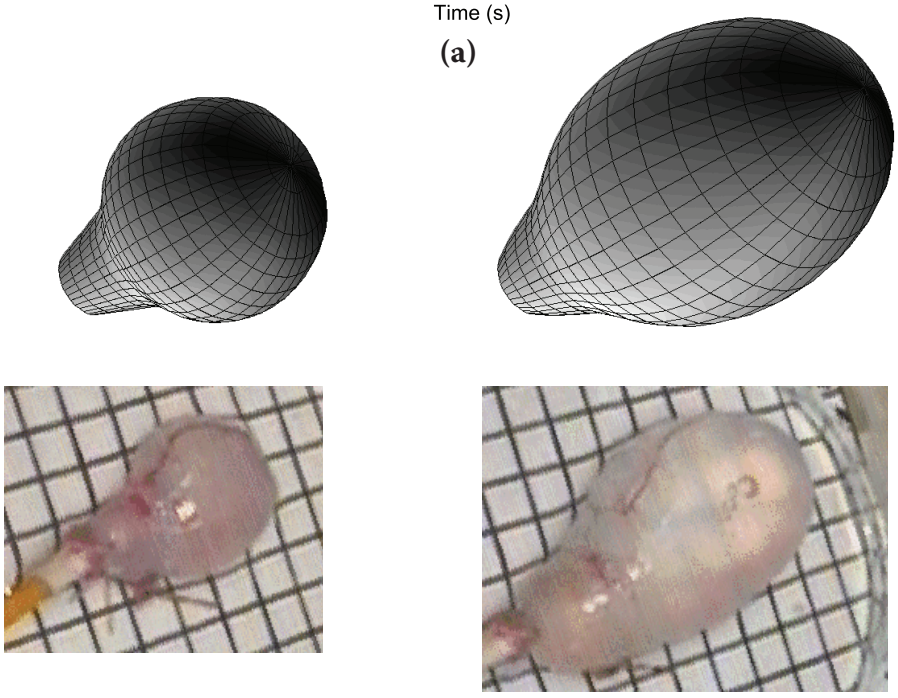

(b)

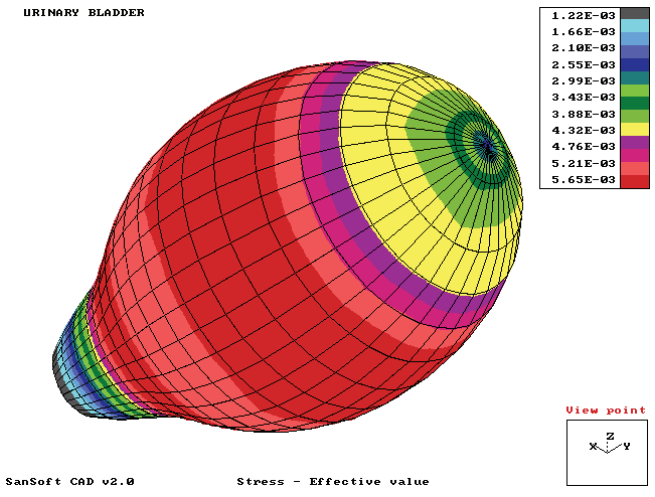

(c)

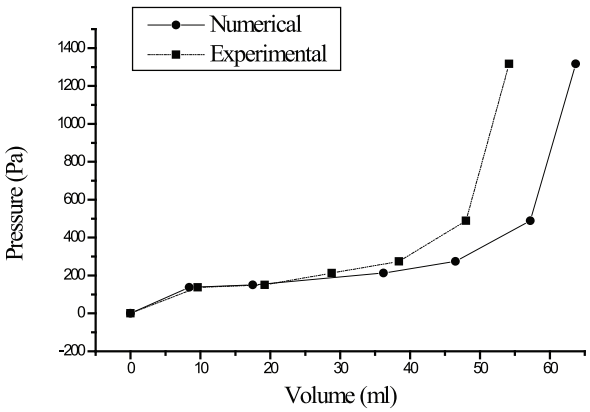

(d)

Fig. 8 Filling of the urinary bladder
(a) Pressure-time relationship
(b) Original and final configurations (computed and experimentally observed)
(c) Stress field in the urinary bladder (final configuration)
(d) Experimental and numerical cystometrograms

the lateral stretches were different for these two cases (Fig. 7d). The lateral (λ_y) and axial (λ_x) stretch values were higher under the same level of stress ($^{t+\Delta t}\sigma_{x}$) when orthotropic material was used because the $^{t+\Delta t}\sigma_{y}\ (\lambda_y)$ curve was considered to lie below the $^{t+\Delta t}\sigma_{x}\ (\lambda_x)$ curve, as seen in Fig. 7e.

In case b), stretching in the x direction produced tensional stress $^{t+\Delta t}\sigma_{y}$ in the y direction. Fig. 7f shows the multistep solutions for both the isotropic and the orthotropic material. In the both cases, we assumed that the following condition was satisfied according to the incompressibility assumption b):

$$\sigma_y = 0.5\sigma_x \tag{42}$$

Fig. 7 g shows the departure (error) of the calculated stress from analytical value for the isotropic material, which was calculated using the following equation

$$\text{Error}\,(\%) = \frac{(\sigma_{xx})_{\text{computed}} - (\sigma_{xx})_{\text{analytical}}}{(\sigma_{xx})_{\text{analytical}}} 100$$

Filling of Urinary Bladder

We analysed urinary bladder response to the filling process. The cystometrogram shown in Fig. 6 was used to calculate the dependence of fluid pressure on time necessary for determination of structural load. In the numerical analysis, we considered continuous filling in addition to pressure loading, as shown in Fig. 8a. A schematic representation of the segment positions used in the experimental investigations is shown in Fig. 4a. The stress-stretch relationships that were employed in the material models are shown in Figs. 4b and 4c, and the coefficients of the models are provided in Table 1. Due to the observed axial symmetry, only one quarter of the structure is modelled, and 162 shell finite elements were included.

Urinary bladder response was calculated using 30 steps, with time step Dt=30s lying in the domain corresponding to the flat parts of the stress-stretch curves and Dt=5s lying in the following domain. The initial configurationwhich used the initial experimentally determined volume value (V0=9.6 ml (numerical V0=5.4 ml)), and the final structure used the final experimentally determined volume value (V0=54.16 ml (numerical V0=43.7 ml)), as shown in Fig. 8b. We noted that the problem was highly nonlinear, both in the geometrical and in the material sense, with stretches of approximately 2.4 λ identified in some regions. The real shapes of the urinary bladder at the initial stage and end of loading that were registered on camera are shown in the same figure. We observed that similar results were identified in the shape and magnitude of the urinary bladder

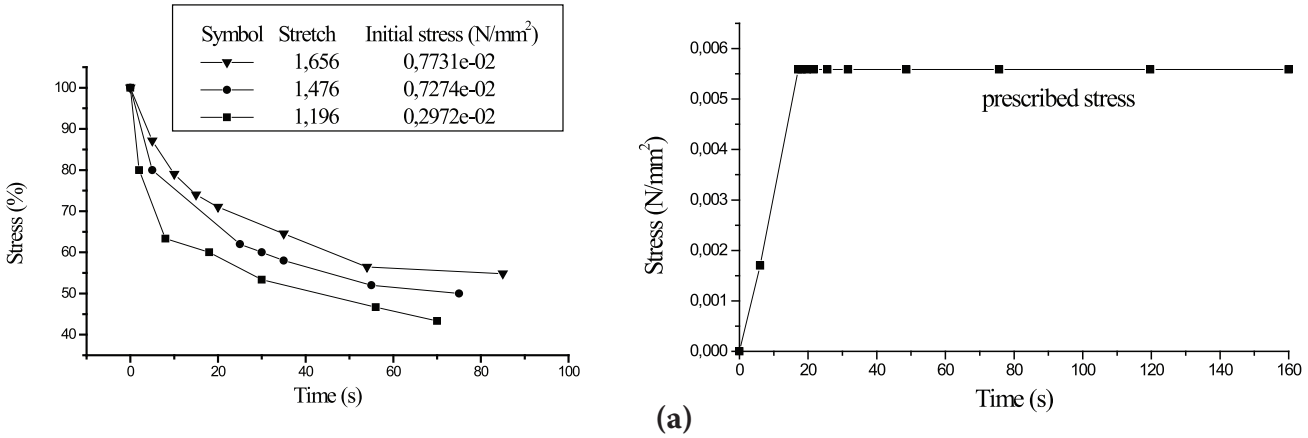

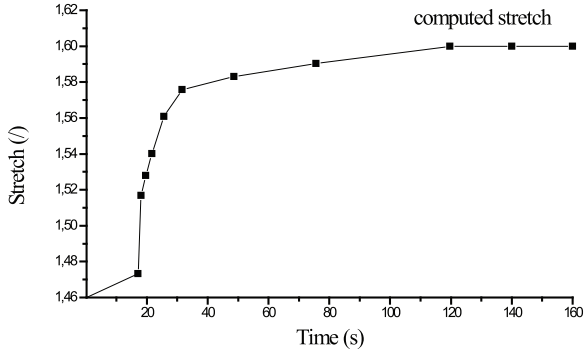

Fig. 9 Uniaxial creep
(a) Experimental relaxation curves
(b) Computed stretch-time relationship

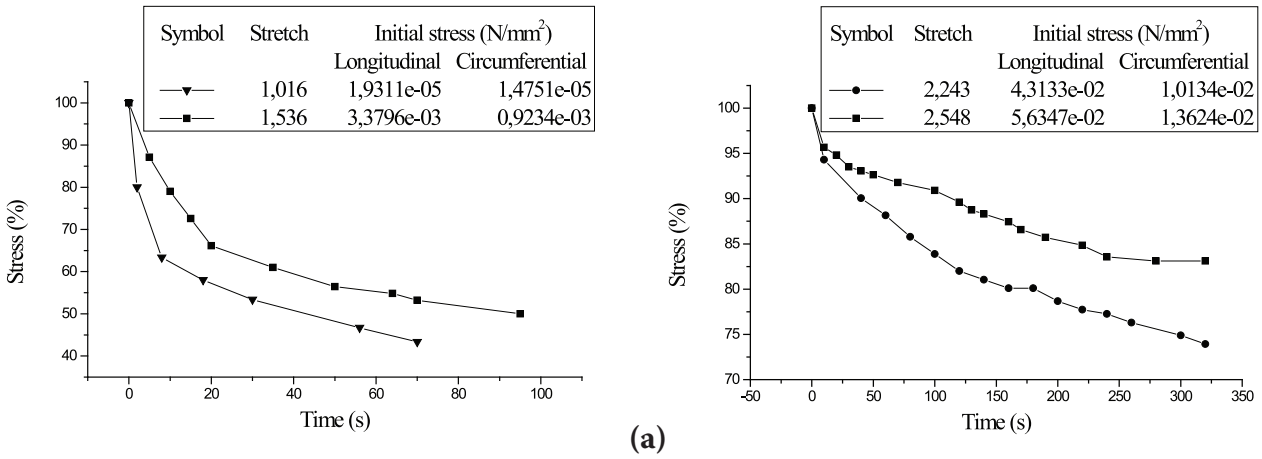

Fig. 10 Creep of urinary bladder
(a) Relaxation curves
(b) Change in volume due to creep at various initial volumes

in the numerical model and the experimental results. The von Mises stress distribution in the wall at the final configuration is presented in Fig. 8c. We noted that the zone of maximum stress was the middle section of the urinary bladder.

Finally, the cystometrograms obtained numerically and experimentally are provided in Fig. 8d. Agreement between numerical and experimental results can be observed based on this figure, verifying the numerical simulation.

Uniaxial Creep.

In this example, we investigated the accuracy of material response prediction using our creep model. In the numerical analysis, we employed the plane stress finite element under constant uniaxial loading conditions. The relaxation curves shown in Fig. 9a were obtained experimentally.

The calculated creep curve, represented as the stretch-time relationship, is shown in Fig. 9b. The figure demonstrates that creep of the material diminished with time, which was also observed experimentally. We observed that the stretch increase that occurred due to creep was relatively small.

Creep of Urinary Bladder.

We calculate the creep of the urinary bladder as a structure, considering, for simplicity, that the material was orthotropic and homogenous with respect to transient loading and creep. In the longitudinal direction, we employed the nonlinear stress-stretch relationship provided by the curve corresponding to segment 9 in Fig. 4b, while for the circumferential direction we used the curve for segment II in Fig. 4c.

The relaxation curves used in the analysis are shown in Fig. 10a, where stress (presented as a percentage of the initial stress observed) is provided as a function of time. The curves for the longitudinal and circumferential directions are the same shape but correspond to different initial stresses, as indicated in the figure.

The internal pressure changed when stepwise filling was employed, as can be seen in the diagram in Fig. 10b. The creep deformation was dominant during the constant pressure-time intervals. The increase in volume that was observed in association with time during creep at various initial bladder volumes corresponded to constant pressures 1,2,...5, as shown in Fig. 10b. We observed that the volume increase was more pronounced under higher stretch conditions (higher initial volumes).

CONCLUSIONS

We have presented the procedures used for experimental determination of the passive mechanical properties of the urinary bladder wall and the results of the numerical analysis performed using state-of-the art modern approaches and ain nonlinear finite element methodology. The stress-stretch curves and the relaxation curves obtained during the experiments were used to formulate the two material models using the analytical form: a) nonlinear model for passive response, and b) creep model. The models were incorporated into the shell finite elements to numerically simulate the transient responses of the urinary bladder under passive and creep conditions.

The results of the numerical simulations demonstrate the possibilities of modelling the complex mechanical behaviour of urinary bladder, which was treated as a thin-walled structure. The proposed methodology provides a solid basis for generating a deeper understanding of the urinary bladder response. This approach may be further generalized to assess the active phase as well, which is the subject of our current research.

REFERENCES

1. Alexander, R. S. Mechanical properties of urinary bladder. Am J Physiol. 1971; 220(5): 1413-1421.
2. Bathe, K. J. Finite Element Procedures. Prentice-Hall, Englewood Cliffs, N. J., 1996.
3. Coolsaet, B. L. R. A., Van Duyl W. A., Van Mastright, R., and Van Der Zwart, A. Visco-elastic properties of the bladder wall. Urol. Int. 1975; 30:16-26.
4. Cvetkovic, A., Milasinovic, D., Peulic, A., Mijailovic, N., Filipovic, N. , , and Zdravkovic N., Numerical and experimental analysis of factors leading to suture dehiscence after Billroth II gastric resection. Computer Methods and Programs in Biomedicine. 2014; 117(2):71-79
5. Damaser, M. S., and Lehman, S. L., The effect of the urinary bladder shape on its mechanics during filling. Journal of Biomechanics. 1995; 28(6): 725-732.
6. Fung, Y. C., Biomechanics-Mechanical Properties of Living Tissues. Springer-Verlag, New York, 1981. pp. 355-381.
7. Griffiths, D. J., Van Mastright, R., Van Duyl, W. A., and Coolsaet, B. L. R. A. Active mechanical properties of the smooth muscle of the urinary bladder. Medical & Biological Engineering & Computing. 1979; 17: 281-290.
8. Kojic, M., Mijailovic, S., Zdravkovic, N. A numerical algorithm for stress integration of a fiber-fiber kinetics model with Coulomb friction for connective tissue. Computational Mechanics, 1998; 21(2): 189-198.
9. Kojic, M., Mijailovic, S., Zdravkovic, N. Modeling of muscle behavior by the finite element method using Hill's three-element model. Int. J. Num. Meth. Engng. 1998; 43: 941-953.
10. Kojic, M., Zdravkovic, N., Mijailovic, S. A numerical stress calculation procedure for a fiber-fiber kinetics model with Coulomb and viscous friction of connective tissue. Computational Mechanics. 2003; 30(3):185-195.
11. Van Mastright, R., Coolsaet, B. L. R. A. and Van Duyl, W. A. Passive properties of the urinary bladder in the collection phase. Medical & Biological Engineering & Computing. 1978; 16: 471-481.
12. Uvelius, B. Isometric and isotonic length-tension relations and variations in cell length in longitudinal smooth muscle from rabbit urinary bladder. Acta Physiol. Scand. 1976; 97: 1-12.